

# PASSIVE, LIGHTWEIGHT THERMAL SOLUTIONS FOR REMOTE RADIO HEAD (RRH) ELECTRONICS

Prathib Skandakumaran, Vikash Khanikar, Martin Smalc, Julian Norley, Brad Reis

GrafTech International Holdings Inc.  
12900 Snow Road, Parma, OH 44130, USA  
Email: [Prathib.Skandakumaran@graftech.com](mailto:Prathib.Skandakumaran@graftech.com)

## ABSTRACT

The ever-increasing size of wireless networks has led to the development of new base station architectures. Traditional telecommunication base stations have baseband and radio-frequency (RF) components mounted inside an air-conditioned hut with co-axial cables transmitting signals to remote antennas. The industry is moving to distributed network and Remote Radio Head (RRH) architectures where the baseband components are digitally connected to a group of RF components mounted on top of antenna towers. Operators who maintain these units typically desire a lightweight, low-volume passive thermal solution. Thermal issues are challenging with power amplifier (PA) powers ranging from 100-200 Watts. Traditional base station heat sinks that cool high-powered PA's are made of a die-cast aluminum material having a low thermal conductivity.

This paper introduces a unique two-phase heat spreader technology to improve the thermal performance of die-cast aluminum heat sinks used in RRH application. Experiments and CFD models were used to compare the thermal performance of baseline aluminum heat sinks to thermal solutions that included an embedded or directly-attach two-phase heat spreader. Results are presented that show a heat sink combined with a two-phase heat spreader solution can provide a 20% reduction in PA temperature or a 17% reduction in heat sink weight.

**KEYWORDS:** Remote Radio Head, RRH, two-phase heat spreader, vapor chamber, heat sink

## NOMENCLATURE

A	cross-sectional area ( $m^2$ )
AHS	Active Heat Spreader
d	AHS vapor section thickness (m)
HS	heat sink
k	thermal conductivity (W/mK)
l'	effective length (m)
L	latent heat of vaporization (J/kg)
p	vapor pressure (Pa)
Q	heat flow (W)
R	thermal resistance ( $^{\circ}C/W$ ) or gas constant
T	temperature ( $^{\circ}C$ )

## Greek symbols

$\mu$	viscosity ( $N\ s/m^2$ )
$\rho$	density ( $kg/m^3$ )

## Subscripts

2, 3, 4	thermocouple locations
amb	ambient
eff	effective
tot	total thermal resistance ( $^{\circ}C/W$ )
v	vapor

## INTRODUCTION

The wireless industry is moving to a Remote Radio Head (RRH) architecture where the baseband components are digitally connected to a group of RF components mounted on top of antenna towers. This approach reduces the RF power requirements from the power amplifier (PA) and improves signal transfer through the use of fiber-optic cables. In addition, a central base station connected to multiple antennas eliminates the need for the redundancy of baseband units, reducing both capital and maintenance costs<sup>(1)</sup>.

However, RRH and tower-mounted electronics raise thermal, reliability, weight, and volume concerns. A typical RRH heat sink, Fig. 1, is large (280 mm x 540 mm base area) and adds significant weight to a tower-mounted RRH system. Thermal issues are more challenging with PA powers ranging from 100-200 Watts. Traditional base stations use a low thermal conductivity ( $\sim 100\ W/mK$ ) cast aluminum heat sink to cool these high-powered PA's. The low thermal conductivity of these cast heat sinks prevents efficient heat spreading of the PA hot-spots into the large base area.



Figure 1. Typical RRH Heat Sink

This paper discusses the use of a thin, flat two-phase or active heat spreader (AHS) to improve the thermal performance of future tower-mounted RRH heat sinks. By improving the heat spreading in the heat sink base, an AHS enables the use of a thinner and lighter heat sink.

## ACTIVE HEAT SPREADERS

The AHS tested is a two-phase heat spreader from GrafTech International Holdings Inc., developed in conjunction with Celsia Technologies<sup>(2)</sup>. An AHS is similar to conventional heat pipes and relies on the evaporation and condensation of water in a closed-system cycle<sup>(3)</sup>. The cycle begins when a small amount of water inside the AHS reaches a sufficient temperature to evaporate and the resulting vapor pressure drop drives the vapor to a cooler condenser section where the vapor condenses. A wick structure in the AHS

serves to return the condensed liquid to the evaporator section where the cycle continues.

An AHS differs from a traditional heat pipe <sup>(4,5)</sup> in that the AHS typically is much thinner and has a much larger external surface area. Thicknesses vary from 1.5-2.5 mm and width and length dimensions can range up to 50 mm and 500 mm, respectively. A thin thermal solution with a large surface area is ideal for RRH applications where space is critical.

Since the AHS is a two-phase spreader, the thermal conductivity will vary depending on a number of parameters, such as heat source size, thermal power, and convection boundary conditions. Traditional heat pipe thermal conductivities are quoted as high as 10,000 – 30,000 W/mK. This conductivity is typically the conductivity of only the vapor region and does not include the conductivity of the other heat pipe components (i.e. wick structure, solid material, and interface resistances). The thermal conductivity of the vapor region of a heat pipe can be calculated using the formula <sup>(6)</sup>:

$$k_v = \frac{L^2 p_v \rho_v d_v^2}{12 R \mu_v T_v^2} \quad (1)$$

where L is the latent heat of vaporization,  $d_v$  is the thickness of the vapor section, R is the gas constant and  $\mu_v$ ,  $\rho_v$ ,  $p_v$  and  $T_v$  are the viscosity, density, vapor pressure and temperature, respectively, of the vapor.

When performing system-level numerical modeling, it is undesirable to model the details of a two-phase spreader; instead a bulk or effective thermal conductivity,  $k_{eff}$ , of the two-phase spreader is preferred. To obtain  $k_{eff}$  for the AHS, experiments were performed, as shown in Fig. 3, where a heat source was attached to the AHS at one end (the evaporator end) and forced air, in a wind tunnel, was blown over the other end (the condenser end). Thermocouple  $T_{AHS}$  was used to monitor the temperature of the face of the evaporator section in contact with the heat source and thermocouples  $T_2$ ,  $T_3$  and  $T_4$  were used to monitor the temperature of the condenser region of the AHS.

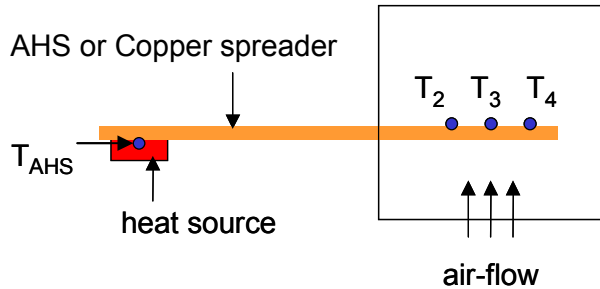


Figure 2. Schematic of AHS and copper heat spreader test setups

The heat source power was varied from 10–45 W and the total thermal resistance,  $R_{total}$ , was calculated using Eq. 2,

$$R_{total} = \frac{T_{AHS} - T_{amb}}{Q} \quad (2)$$

where  $T_{AHS}$  is the maximum temperature on the AHS,  $T_{amb}$  is the inlet temperature of the air in the wind tunnel, and Q is the heat flow.

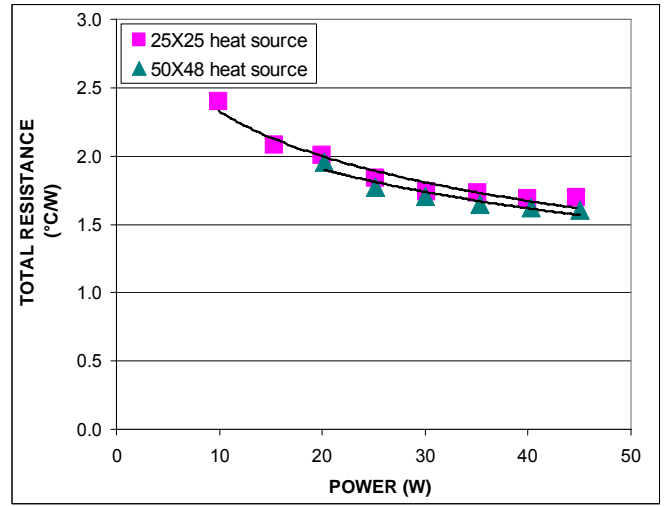


Figure 3. Total Thermal Resistance of AHS tested for a Fixed Air Flow Rate

As thermal power increases, there is an increase in vapor pressure that results in lower total thermal resistance, as shown in Fig. 3. As shown, similar thermal performance was seen for heat source areas of both 25 mm x 25 mm and 50 mm x 48 mm. In addition, it was observed that the thermal performance of the AHS improved significantly at temperatures above 50 °C when the pressure and density of water vapor increase sharply.

To calculate the effective thermal conductivity of the AHS, only its thermal resistance is needed, independent of the convection thermal resistance. The thermal resistance of the AHS,  $R_{AHS}$ , is defined from the maximum AHS evaporator temperature,  $T_{AHS}$ , and the average temperatures  $T_2$ ,  $T_3$  and  $T_4$  on the condenser surface of the AHS using,

$$R_{AHS} = \frac{T_{AHS} - AVG(T_2, T_3, T_4)}{Q} \quad (3)$$

To apply this one-dimensional formula to the experimental results, an effective length,  $l'$ , was calculated. A copper spreader with the same dimensions as those of the AHS was tested and the effective length was calculated from Eq. 4 using the known thermal conductivity of copper.

$$k_{eff} = \frac{l'}{R_{AHS} A} \quad (4)$$

This effective length, which represents the length from the evaporator to the condenser section of the AHS, was then used to compute the effective thermal conductivity of the AHS as a function of thermal power, as shown in Fig. 4.

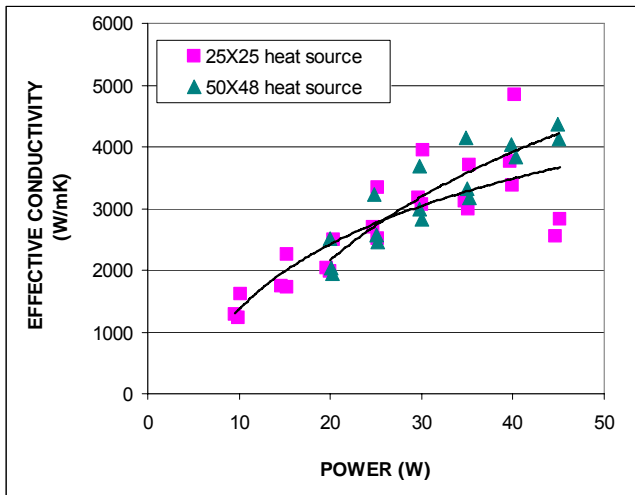


Figure 4. Effective conductivity of a 50 mm X 240 mm AHS for three different air-flow rates

The effective thermal conductivity of an AHS may not be as high as that of a conventional heat pipe. One reason is the effective conductivity includes the thermal resistance of all the components of the AHS (its exterior surfaces, wick structure and vapor spacer) and is not just the result of the vapor thermal conductivity value calculated in Eq. 1. Also, vapor thermal conductivity scales with the square of the vapor section thickness. Therefore, the AHS effective thermal conductivity should not be the only parameter considered when evaluating the thermal performance; the large surface area and the small thickness of the AHS are unique added advantages.

In heat sink applications where base spreading is needed, a two-phase heat spreader base may not always improve overall performance when compared with a solid metal base<sup>(7)</sup>. Depending on its thermal conductivity, base thickness and base area, a solid base may outperform a two-phase spreader base. In the RRH application, where the heat sink base is large (280 mm x 450 mm) and has a low thermal conductivity, there is a benefit to using an embedded two-phase spreader if the base thickness is less than 10 mm. In this paper, tests and CFD models will be used to identify at what thickness a two-phase heat spreader improves the performance of cast and extruded aluminum heat sinks used in RRH applications.

#### TEST SETUP AND PROCEDURE

Experiments were performed using 4 different RRH heat sink configurations (Fig. 5):

- 4 mm thick baseline aluminum heat sink,
- 8 mm thick baseline aluminum heat sink,
- 4 mm thick baseline aluminum heat sink + embedded AHS,
- 4 mm thick baseline aluminum heat sink + direct-attach AHS.

The AHS was located in the center of the heat sink and its length dimension was oriented along the length of the fins. The embedded AHS and direct-attach AHS solutions used a 0.127 mm thick phase-change material as a thermal interface between the AHS and the heat sink. The flatness of the AHS enabled the direct attachment of the AHS to the external surface of the heat sink, eliminating the need for a machining step commonly used with embedded heat pipe solutions.

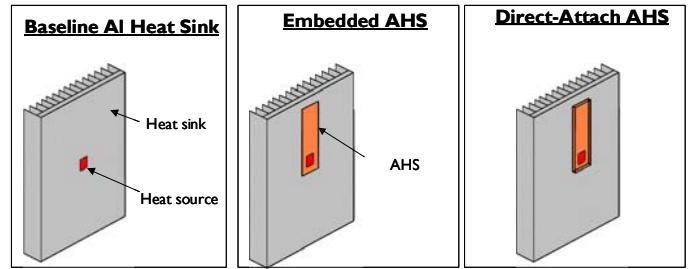


Figure 5. RRH heat sink solutions: Baseline aluminum, embedded AHS and direct-attach AHS

Because it was readily obtainable, a heat sink made from extruded aluminum alloy 6063, with a thermal conductivity of 187 W/mK, was used in these tests. All of the tested heat sinks had the same fin dimensions and a base area of 280 mm x 540 mm. The test setup, shown in Fig. 6, consisted of the heat sink with fins aligned vertically and its base pressed against a heat source by a clamp mechanism that provided contact pressure of 90 psi on the heat source.

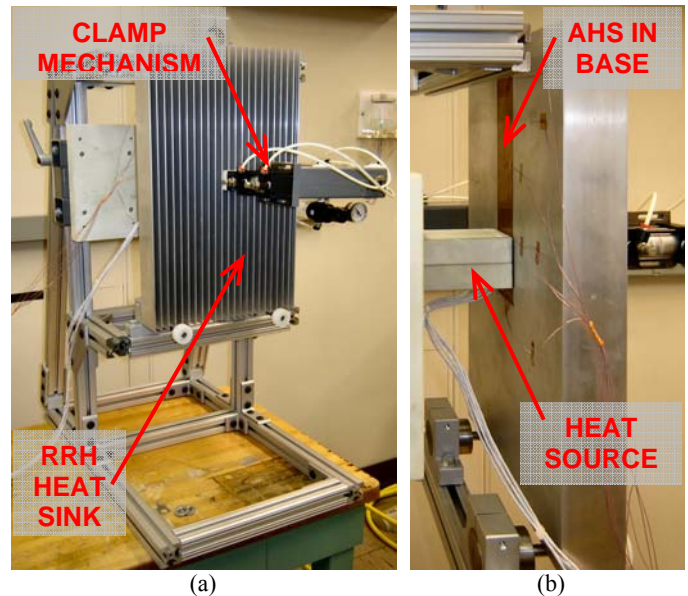


Figure 6. RRH Heat Sink Test Setup, a) RRH Clamped to Test Frame, b) Rear of RRH Heat Sink showing Heat Source and AHS Embedded in Base

The heat source provided a uniform, controlled and constant one dimensional heat flux from the flat heating surface at its end. It consisted of electrical heating elements embedded in a long, rectangular aluminum block with a heating surface 25 mm x 25 mm square. This assembly was encased in an insulated housing to minimize heat loss and ensure essentially one dimensional heat flow along the length of the block. A graphite TIM<sup>(8)</sup> was used between the spreader and the heating surface. Five Resistance Temperature Detectors (RTDs), evenly spaced along the length of the block, were used to measure the temperature gradient in the block. The block was made from 6063 aluminum with a thermal conductivity of 187 W/mK. The heat flow into the heat sink was determined from the temperature gradient, thermal conductivity and cross sectional area of the block.

Temperature data was measured with an Agilent 34907A Data Acquisition Unit equipped with Agilent 340901A Twenty Channel

Multiplexer Cards. The heat sources were powered with an Agilent 6655A Programmable DC Power Supply. A custom heat control and data acquisition program was written using Agilent Vee Pro 6.0 software. This program monitored temperatures and controlled heat flow using a PID control loop to adjust the electrical power to the heater. It also recorded spreader temperature data automatically after thermal equilibrium was established.

The heat sinks were tested at 75 Watts of thermal power in a natural convection environment. Type T thermocouples were attached to the heat sink. One thermocouple was located on the heat sink base directly above the heat source and was used to obtain the maximum heat sink temperature. The source had a 1.5 mm wide X 1 mm deep slot cut into its contact surface to provide clearance for this thermocouple. This temperature was used to compare the performance of the various heat sink configurations. An aluminum plate with a thermocouple bonded to it was located adjacent to the test fixture to measure ambient temperature.

### RESULTS AND DISCUSSION

Fig. 7 shows the maximum heat sink temperatures obtained measured on the four heat sinks. The 4 mm base heat sink exhibited the highest temperature while the 8 mm base heat sink had the lowest temperature, showing that increasing base thickness provides additional cross-sectional area for heat spreading. The embedded AHS and direct-attach AHS solutions improved the bulk thermal conductivity of the base and these solutions exhibited lower base temperatures than the 4 mm base heat sink. However, these two solutions did not perform thermally as well as the 8 mm base heat sink. Clearly, in these extruded aluminum heat sinks (having a thermal conductivity of 187 W/mK), the base thickness was the dominant parameter controlling thermal performance. Unless weight or form-factor is important, the thicker base provides sufficient heat spreading. However, there are two cases where the AHS solution works well: 1) on a thin base (selected because of weight or form-factor restrictions), and 2) on a heat sink made from a lower thermal conductivity aluminum casting alloy.

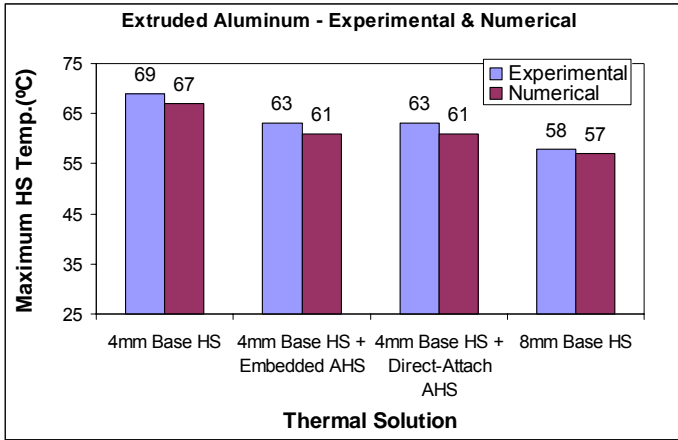


Figure 7. Extruded Aluminum Heat Sink Solutions: Experimental Results and CFD Modeling Results

Many RRH heat sinks are manufactured from low thermal conductivity (100 W/mK) aluminum casting alloys as opposed to higher thermal conductivity (200 W/mK) aluminum extrusion alloys. The advantage of the cast alloys over extruded aluminum is the ability to cast in fine features such as EMI cavities for shielding of PCB board components. To determine the effect of using an AHS

solution in the base of a cast aluminum heat sink, CFD simulations were performed using commercially-available CFD software [9].

The CFD model was validated using the experimental results for the extruded aluminum heat sink tests shown in Fig. 7. As shown, there is good agreement between the numerical and experimental results. The CFD model was then used to determine the performance of the AHS solution on cast aluminum heat sinks having a thermal conductivity of 100 W/mK. These results are shown in Fig. 8. As shown, both of the AHS solutions on the 4 mm base, have a lower maximum temperature than the 8 mm base heat sink. The computed temperature distributions of the baseline cast aluminum heat sink and the cast aluminum heat sink with an embedded AHS solution are shown in Fig. 9. The AHS solution spreads the heat from the 75 Watt heat source throughout the base and reduces the maximum heat sink temperature.

In addition to the thermal advantage, use of an AHS provided a significant weight advantage as shown in Table 1. The Embedded AHS solution showed a ~17% reduction in weight compared to the 8 mm thick Base HS.

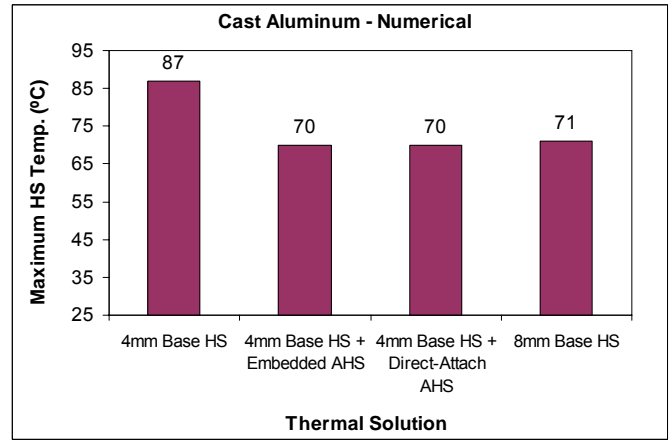


Figure 8. Cast Aluminum Heat Sink Solutions from CFD Modeling

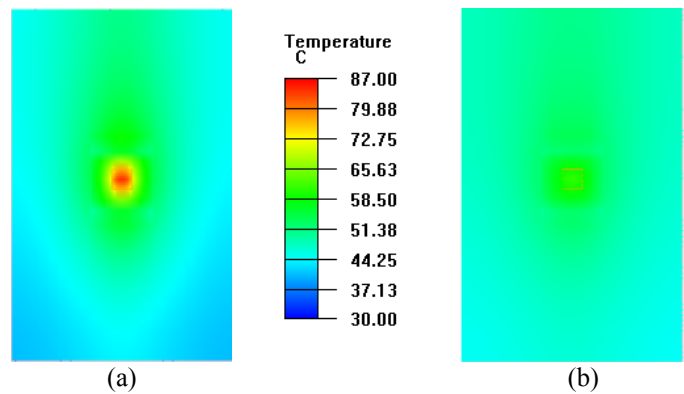


Figure 9. Temperature Profiles from CFD Modeling: (a) Cast Aluminum, (b) Cast Aluminum + Embedded AHS

Table 1. RRH Heat Sink Weights

Thermal Solution		Weight (g)
1	4mm Base HS	6,530
2	4mm Base HS + Embedded AHS	6,550
3	4mm Base HS + Direct-Attach AHS	6,620
4	8mm Base HS	7,890

### NICKEL PLATING

In outdoor applications, components and metallic materials are typically nickel plated to protect them from corrosion. To test the effect of the nickel-plate coating on the AHS performance, a 50 mm x 240 mm x 2 mm AHS was plated with 50 µm thick nickel using an electroless nickel-plating process. A thermal experiment was then performed to quantify the performance difference between the non-plated AHS and a nickel plated AHS.

Both spreaders were tested in a vertical orientation in natural convection on a 25 mm x 25 mm heat source. A black paint coating was applied to both spreaders to maintain the same emissivity. Tests were performed using a range of thermal powers and the results, in Fig. 10, showed little difference between the two spreaders.

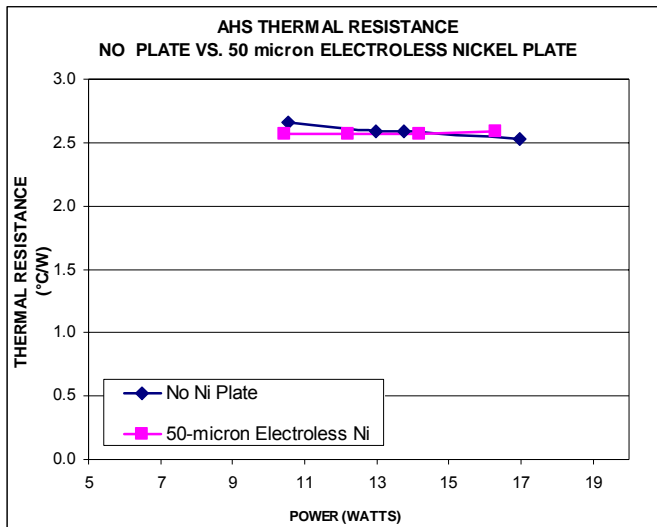


Figure 10. Baseline Thermal Resistance Measurements

### CONCLUSIONS

The performance of a two-phase Active Heat Spreader (AHS) was described. The AHS effective conductivity was calculated and showed promise for applications where solid metal spreading was not sufficient. The flatness, thinness and large surface area of the AHS enable its use in applications where form factor and weight are critical, such as in a RRH heat sink.

This study identified spreading in the heat sink base as a thermal bottleneck in large RRH heat sinks. Two AHS solutions were

investigated: embedding the AHS into a heat sink base and directly attaching the AHS to the heat sink base. Experiments and CFD analysis quantified the effectiveness of these solutions. The AHS solutions show a 17 °C reduction in temperature compared with a cast aluminum heat sink when the base thickness was 4 mm. The embedded solution provided similar thermal performance to a cast aluminum heat sink with an 8 mm base at a 1.3 kg or 17 % lower weight. The additional of a 50 µm thick, electroless nickel plated layer to the AHS spreader did not affect thermal performance.

### ACKNOWLEDGMENTS

The authors wish to acknowledge George Meyer and Celsia Technologies Inc. for their assistance, technical leadership and cooperation in providing the base AHS technology described in this paper. We also wish to acknowledge the assistance of Terri Gold for proofreading and finalizing the manuscript.

### REFERENCES

- [http://www.siemens.com/Daten/siccom/HQ/COM/Internet/Mobile\\_Networks/WORKAREA/com\\_mnen/templatedata/English/file/binary/RRH\\_RS\\_0106\\_1351002.pdf](http://www.siemens.com/Daten/siccom/HQ/COM/Internet/Mobile_Networks/WORKAREA/com_mnen/templatedata/English/file/binary/RRH_RS_0106_1351002.pdf)
- eGRAF® CL-1000 is a trademark of GrafTech International Holdings Inc. and developed in conjunction with Celsia Technologies
- Meyer, G.A. and Saums, D.L., Practical Application Guidelines for Vapor Chambers for Electronics Thermal Management, IMAPS 2007, San Jose, CA.
- Peterson, G.P., An Introduction to Heat Pipes – Modeling, Testing and Applications, John Wiley & Sons, Inc.
- Dunn, P. D. and Reay, D. A., Heat Pipes, Pergamon, Elsevier Science, Inc.
- Prasher, R., A Simplified Conduction Based Modeling Scheme for Design Sensitivity Study of Thermal Solution Utilizing Heat Pipe and Vapor Chamber Technology, Journal of Electronic Packaging, September 2003, Vol. 125.
- Sauciuc, I., Chrysler, G., Mahajan, R., Prasher, R., Spreading in the Heat Sink Base: Phase Change Systems or Solid Metals??, IEEE Transactions on Components and Packaging Technologies, Vol. 25, No. 4, December 2002.
- eGRAF® HITHERM™ 2510, a trademark of GrafTech International Holdings Inc.
- Icepak™ 4.3.10 is a trademark of ANSYS, Inc.